

Machine-learning for photoplethysmography analysis: Benchmarking feature, image, and signal-based approaches

Mohammad Moulaeifard¹, Loic Coquelin², Mantas Rinkevičius³,
 Andrius Sološenko³, Oskar Pfeffer⁴, Ciaran Bench⁵, Nando
 Hegemann⁴, Sara Vardanega⁶, Manasi Nandi⁶, Jordi Alastruey⁶,
 Christian Heiss⁷, Vaidotas Marozas³, Andrew Thompson⁵, Philip J.
 Aston^{5,8}, Peter H. Charlton⁹, and Nils Strodthoff¹

¹Carl von Ossietzky Universität Oldenburg, Oldenburg, Germany

²Laboratoire national de métrologie et d'essais, Paris, France

³Biomedical Engineering Institute, Kaunas University of Technology,
 Kaunas, Lithuania

⁴Physikalisch-Technische Bundesanstalt, Berlin, Germany

⁵National Physical Laboratory, Teddington, United Kingdom

⁶King's College London, London, United Kingdom

⁷University of Surrey, Surrey, Guildford, United Kingdom

⁸Department of Mathematics, University of Surrey, Guildford,
 United Kingdom

⁹Department of Public Health and Primary Care, University of
 Cambridge, Cambridge, United Kingdom

Abstract

Photoplethysmography (PPG) is a widely used non-invasive physiological sensing technique, suitable for various clinical applications. Such clinical applications are increasingly supported by machine learning methods, raising the question of the most appropriate input representation and model choice. Comprehensive comparisons, in particular across different input representations, are scarce. We address this gap in the research landscape by a comprehensive benchmarking study covering three kinds of input representations, interpretable features, image representations and raw waveforms, across prototypical regression and classification use cases: blood pressure and atrial fibrillation prediction. In both cases, the best results are achieved by deep neural networks operating on raw time series as input representations. Within this model class, best results are achieved by modern convolutional neural networks (CNNs). but depending on the

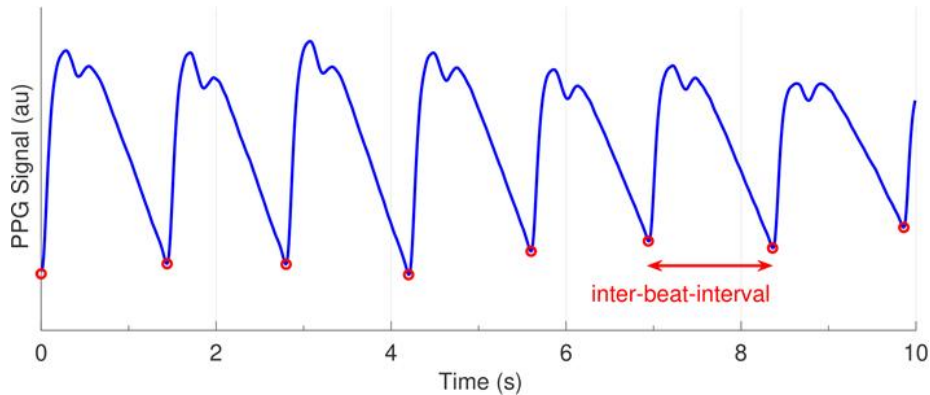


Figure 1: An exemplary PPG signal showing a pulse wave for each heartbeat. Pulse onsets, representing individual heartbeats, are shown as red circles. An inter-beat interval is labeled, corresponding to the time between consecutive heartbeats (adapted from [7]).

task setup, shallow CNNs are often also very competitive. We envision that these results will be insightful for researchers to guide their choice on machine learning tasks for PPG data, even beyond the use cases presented in this work.

1 Introduction

PPG is one of the most commonly used wearable sensing techniques. It consists of projecting light onto the skin and measuring the amount of light that is reflected back or transmitted through the underlying tissues. Its simplicity, non-invasive nature, and ability to deliver multiple physiological parameters make it particularly attractive [1, 2]. As a result, PPG has been integrated into a range of clinical devices, such as pulse oximeters, as well as consumer wearable devices including smartwatches.

The PPG signal measures the fluctuations in blood volume in the skin’s microvascular bed which occur with each heartbeat. Figure 1 shows an exemplary PPG signal: the shape of the pulse wave contains information relating to the heart and vasculature, including blood pressure; and the inter-beat intervals are related to heart rhythm [3]. The time delay between the electrical activation of the heart and the arrival of the corresponding pulse wave at a peripheral site where PPG is measured has been used to predict blood pressure. There are generally two approaches to analysing PPG signals (1): (i) using signal processing to extract features relating to pulse wave shape or inter-beat-intervals; and (ii) using deep learning techniques to analyse PPG signals or their image-based representations [4]. Over the past few years, deep learning techniques have become widely used [5, 6].

In this work, we investigate two widely considered clinical applications for PPG analysis: atrial fibrillation (AF) classification as a prototypical classification task and cuffless blood pressure (BP) estimation as a prototypical regression task. AF is the most common sustained cardiac arrhythmia and confers a five-fold increase in stroke risk [8]. AF is characterised by irregular and often very rapid heart rhythm. PPG provides an attractive approach to identifying AF because it is widely used in consumer wearables, and because it can detect each heart beat, it can provide measures of the heart rhythm. In the case of AF, the time intervals between heart beats are irregular. BP is one of the most widely used physiological measurements. It is a key marker of cardiovascular health; a valuable predictor of cardiovascular events; and is essential for the selection and monitoring of antihypertensive (BP lowering) treatments [9]. PPG-based blood pressure estimation provides a potential approach to monitor BP unobtrusively in daily life. The rationale behind selecting two prototypical, but very different use cases is to identify general patterns that could guide practitioners in the field even beyond the two investigated use cases.

While many prediction models have been put forward for the two considered prediction tasks at hand, benchmarking results are typically presented within a set of prediction models operating on a single kind of input modality or a comparison is carried out against previously reported results from the literature. However, the latter rely on matching the experimental setup as closely as possible, where deviations from this setup severely limit the comparability of the results. The current lack of like-to-like comparisons is an important gap in the research landscape, that we aim to address with this submission.

In this work, we address the following research questions: How do state-of-the-art machine learning models operating on different input representations compare? Are there universal patterns in terms of best-performing input representations or model architectures across different prototypical classification and regression use cases? As our main technical contribution, we put forward a like-to-like benchmarking of a comprehensive set of state-of-the-art algorithms covering three kinds of input representations on two large-scale datasets for a prototypical classification task (AF classification) and two different variants of a prototypical regression (BP regression) task.

2 Related Work

Machine Learning Approaches. Typically, all approaches for clinical prediction tasks based on PPG data rely on a combination of signal processing and machine learning, where the precise focus varies considerably across different approaches. At one end of the spectrum, approaches relying on clinically interpretable features focus heavily on signal processing to extract meaningful features and typically use comparably simple classification/regression models to perform the prediction. At the other end of the spectrum, deep learning methods using raw time series as input with as little signal processing as possible rely

on complex prediction models to extract and process meaningful features by themselves. In between, there are classifiers based on image-representations, that leverage signal processing tools to turn raw waveforms into image representations and then most commonly also rely on deep learning models to perform the prediction.

Time Series Models. Recent advancements in deep learning have significantly impacted healthcare by enabling complicated analysis of raw physiological data. These models are particularly effective in estimating BP and detecting AF, among other applications. The key advantage of deep learning is its ability to recognize complicated patterns directly from raw data such as electrocardiogram (ECG) and PPG signals, eliminating the need for extensive manual feature development [10, 11]. They provide an effective means to learn the complex, nonlinear underlying relationship between PPG signals and various physiological parameters, without the need to define a convenient analytical form for such a transformation. Consequently, deep learning architectures such as convolutional neural networks (CNNs) and recurrent neural networks (RNNs) have shown remarkable performance in BP estimation, by capturing the temporal and spatial nuances inherent in raw physiological signals [12]. Similarly, deep learning models have demonstrated significant potential in detecting AF from raw ECG signals. The authors of [13] developed a deep learning model employing a CNN to detect AF from single-lead ECG recordings. Their model demonstrated high accuracy, underscoring the potential of deep learning in the detection of arrhythmias. Similarly, [14, 15, 16] implemented deep learning approaches using CNNs on PPG signals for AF detection. These approaches yielded results that were competitive with ECG-based methods, thereby demonstrating the feasibility of utilizing PPG signals for AF detection. End-to-end deep learning frameworks that process raw ECG data to generate AF predictions have simplified and improved the accuracy of AF detection.

Feature-Based Models. Besides working on raw data, another possibility to solve classification or regression tasks on PPG data is to establish machine learning models operating on clinically interpretable PPG features. These features include features based on pulse morphology, e.g. PPG pulse wave features such as the systolic peak, the diastolic peak or pulse duration and PPG derivative features (6,17), and irregularity features based on measures of randomness, variability and complexity in the inter-beat-intervals that can be determined from the PPG [17, 18]. These clinically interpretable PPG features are used for BP estimation (see below), AF detection (see below) and other questions related to the cardiovascular system, e.g. the assessment of arterial stiffness [19]. In addition, PPG signals show sometimes a strict periodic behaviour or, in general, a quasi-periodic behaviour. This motivates the use of features from Fourier- [20], Wavelet- [21] or Hilbert-Huang- [22] Transformations for training models. Such models are defined for BP estimation and AF detection. In related work, features from Fourier-Transformation are used to define models for the detection of aneurysms [23] or stenoses [24]. As PPG signals are in general not periodic, but quasiperiodic, one might expect better results with Wavelet- or

Hilbert-Huang-transformations.

Image-Based Models. Image-based models, such as those using the Continuous Wavelet Transform (CWT), convert physiological signals into visual representations, enabling deep learning to analyze, classify, and estimate physiological parameters. The CWT is a powerful tool for analyzing localized variations of power within a time series signal. Unlike the Fourier Transform, which provides a global frequency representation, CWT can provide a time-frequency representation that preserves the temporal localization of features. CWT based scalograms have already been used for PPG signal transformation to classify BP (Normal, Prehypertension, Stage 1 hypertension and Stage 2 hypertension) [25, 26], estimate heart rate variability (HRV) and signal quality [27] as well as to detect atrial fibrillation [15].

3 Materials and Methods

3.1 Datasets

This study utilized the PPG data contained in the VitalDB dataset [28] for BP estimation and in the DeepBeat dataset [29] for the AF detection task.

Table 1: Characteristics of the VitalDB subsets used for BP estimation.

Subset	VitalDB ‘Calib’	VitalDB ‘CalibFree’
Train (samples / subjects)	418986 / 1293	416880 / 1158
Validation (samples / subjects)	40673 / 1293	32400 / 90
Test (samples / subjects)	51720 / 1293	57600 / 144
Age (mean \pm SD)	58.98 \pm 15.03	58.89 \pm 15.07
Sex (M%)	57.69	57.91
SBP (mmHg, mean \pm SD)	115.48 \pm 18.92	115.47 \pm 18.91
DBP (mmHg, mean \pm SD)	62.92 \pm 12.08	62.93 \pm 12.06

VitalDB dataset. The VitalDB dataset includes ECG, PPG, and invasive arterial blood pressure (ABP) signals collected using patient monitors from surgical patients [30]. Wang et al. (26) published the pre-processed VitalDB dataset as a subset of the PulseDB dataset, from which we use the PPG signals of 10s length with sampling frequency of 125 Hz, and reference systolic BP (SBP) and diastolic BP (DBP) values derived from the ABP signals. The dataset supports both calibration-based (in which train and test datasets share subjects) and calibration-free (in which train and test sets do not share subjects) testing approaches, which are essential for assessing the generalizability of BP estimation models. We refer to the first scenario as **VitalDB ‘Calib’** and to the second scenario as **VitalDB ‘CalibFree’**. To ensure comparability with literature

results, we keep the original test sets intact but split the original training sets into training, validation and calibration sets, where the latter is not considered in this study, mimicking the way the respective test sets were created, i.e., defining validation sets with/without patient overlap for VitalDB ‘Calib’/‘CalibFree’. In Table 1, we summarize the two considered subsets, where one sample corresponds to a segment of 10s length.

Table 2: Characteristics of the DeepBeat subsets used for AF classification.

Dataset	DeepBeat (AF classification)			
	AF	Non-AF	Data Ratio	AF Ratio
Train (samples / subjects)	40603 / 50	65646 / 38	0.78	0.38
Validation (samples / subjects)	5800 / 19	9456 / 7	0.11	0.38
Test (samples / subjects)	5797 / 19	9580 / 5	0.11	0.37

DeepBeat dataset. For the AF classification task, we leveraged the DeepBeat dataset [29]. The dataset comprises more than 500,000 25-second, 32 Hz PPG segments, henceforth referred to as samples, from 175 individuals (108 with AF, 67 without). PPG signals were collected using a wrist-based PPG wearable device from cohorts of participants before cardioversion, patients undergoing an exercise stress test, and during daily life [29]. In the original publication [29], due to uneven AF/non-AF distribution across splits, performance metrics were overestimated, and the strong test scores did not reflect equivalent success on the validation and training sets. To address these issues, we implemented a new data split. We ensured no overlap between sets by redistributing subjects, thereby eliminating the redundancy present in the original dataset (Table 2). This revised split maintains an equal AF/non-AF ratio across the training, validation and test sets, providing a more reliable representation and enhancing the robustness of our model evaluation. (for more details please refer to the Supplementary Material).

3.2 Performance Evaluation and Metrics

To keep the main text concise, we summarize our evaluation methods here. For a detailed explanation of the procedures and metrics used, please refer to the Supplementary Material.

Blood Pressure Estimation. We evaluate BP predictions using the Mean Absolute Error (MAE) and Mean Absolute Scaled Error (MASE), comparing

model outputs against a baseline that predicts the training set median. Metrics are reported separately for systolic and diastolic pressures.

We also provide the grading (A, B, C, D) based on IEEE 1708a-2019 standard [31] which are calculated based on the difference between the device or model’s BP predictions and the reference (cuff-based) measurements;

- **Grade A:** Errors ≤ 5 mmHg
- **Grade B:** Errors between 5 and 6 mmHg and equal to 6 mmHg
- **Grade C:** Errors between 6 and 7 mmHg and equal to 7 mmHg
- **Grade D:** Errors > 7 mmHg

Atrial Fibrillation Detection. AF detection performance is assessed using standard metrics—sensitivity, specificity, receiver operator characteristic (ROC) area under curve (AUC), F1 score, and Matthews correlation coefficient (MCC). Classification thresholds are adjusted to meet desired sensitivity/specificity criteria, with a default threshold of 0.5 for the F1 score and optimized thresholds for other metrics. We explore two different threshold choices by fixing the threshold such that either sensitivity or specificity exceeds 0.8.

3.3 Prediction models

In our study, we explore the use of three different input representations — time series, feature-based, and image-based approaches—each providing unique advantages in capturing the underlying physiological information. We consider several architectures, each designed to process either raw signals, extracted features, or visual representations to accurately estimate BP values and classify heart rhythms.

Baseline Models. On VitalDB CalibFree, the baseline model (used for BP estimation) predicts BP by outputting the median SBP/DBP value of the blood pressure data inferred from the training set for any given input, providing a straightforward reference for evaluating the performance of more advanced predictive models. On VitalDB Calib, we use the subject-specific median calculated as prediction on the test set.

Raw Time Series Models. For both BP estimation and AF detection, deep learning architectures such as CNNs, RNNs, and TCNs have been used to process raw ECG or PPG sequences to capture complex temporal patterns, directly predicting continuous values for regression or output probabilities for classification. The specific models used in this study were:

- **LeNet1d:** A one-dimensional CNN adapted from the original LeNet architecture for feature extraction from raw ECG/PPG time-series data [32].
- **Inception1d:** A 1D adaptation of the Inception architecture that uses parallel convolutional layers to capture multi-scale temporal features [33].

- **XResNet1d50/101:** Deep residual networks modified for 1D data, incorporating group normalization and selective kernel sizes to learn hierarchical features from physiological signals. [34].
- **XResNet1d50+GNLL:** This model explores the XResNet50d with a Gaussian Negative Log Likelihood Loss (GNLL) instead of the conventional MAE loss as proposed in [35].
- **AlexNet1d:** A one-dimensional variant of AlexNet that processes time series data through convolutional and pooling layers for regression and classification tasks [36].
- **MiniRocket:** A nearly deterministic transform using dilated convolutions and a linear classifier, offering fast and effective feature extraction from time-series data [37].
- **Temporal Convolutional Networks (TCNs):** Networks using dilated causal convolutions and residual connections to capture long-range dependencies in sequential physiological signals [38].

We can roughly categorize the considered models into complex/deep models (Inception1D, XResNet1d50, XResNet1d101) and simple/shallow models (LeNet1d, AlexNet1d, MiniRocket, TCNs).

Feature-Based Models. Clinically interpretable features are extracted from PPG signals—such as pulse morphology metrics for BP estimation and irregularity measures for AF detection—and fed into machine learning algorithms to perform regression or classification tasks with clearer interpretability. The specific models and techniques used in this study were:

- **Clinically interpretable features (CIF):** CIF for BP includes features such as systolic peaks, diastolic peaks, pulse duration, and pulse morphology metrics [39]. These features reflect vascular health, haemodynamic dynamics, and arterial compliance, making them well-suited for modeling BP. CIF for AF comprises features related to rhythm irregularity, such as randomness [40], variability [41, 42], and complexity in inter-beat-intervals [43]. These features highlight the irregular heart rhythms characteristic of atrial fibrillation. The full list of features is described in the supplementary material. These features are combined with the following prediction models:
- **Multi-layer perceptron (MLP):** An MLP is a fully connected feedforward neural network that maps input features to target outputs through multiple layers of neurons.
- **Gaussian Process Regression (GPR):** A non-parametric regression method that models complex relationships between PPG features and BP, providing probabilistic predictions [44].
- **Wavelet Transformation:** A Wavelet-based method such as Wavelet Packet Decomposition using the Discrete Wavelet Transform [45] is applied

to the raw PPG signal. This transformation decomposes the signal into time-frequency components, extracting features that capture both transient and long-term patterns in the data. It should be noted that Wavelet + Multi-Layer Perceptron (MLP) forms a pipeline where the wavelet transform serves as a sophisticated feature extractor, and the MLP functions as the predictive model utilizing those features.

Image-Based Models: One-dimensional signals can be converted into two-dimensional images which capture the essence of the signal in a compact domain. Traditional image recognition CNNs can then be used with these image inputs. There are different ways of converting signals to images, but this study only used the following approach:

- **Continuous Wavelet Transform (CWT) Scalograms:** PPG signals are transformed into time-frequency images derived from PPG signals that capture localized signal variations (26). The CWT-based images are used as inputs for ResNet18 models.

For more details on these models and their implementations, please see the Supplementary Material.

4 Results

4.1 Blood Pressure Estimation

Tables 4 & 3 display the results of blood pressure (SBP/DBP) prediction using different deep learning models based on VitalDB Calib and VitalDB CalibFree datasets, respectively. The baseline models achieved MAEs of 14.87 and 9.43 mmHg for SBP and DBP respectively on CalibFree, and 10.72 and 5.78 mmHg respectively on Calib. On Calib, the per-subject baseline performed substantially better than the global baseline (10.72 and 5.78 mmHg vs. 14.91 and 9.52 mmHg respectively).

Model performance varied between models and tasks. On CalibFree, almost all models provided an improvement over baseline for both SBP and DBP (the only exception being the Inception1d SBP model). However, the level of improvement was moderate at best, with the lowest MASEs of 0.83 for both SBP and DBP achieved by XResNet1d50, indicating 17% reductions in MAE in comparison to baseline. This resulted in at best 26% of SBP estimates and 40% of DBP estimates falling into the top grade (*i.e.* errors of <5 mmHg). On Calib, there was greater variation in model performances, with XResNet1d50+GNLL achieving the lowest MASEs of 0.73 and 0.87 for SBP and DBP respectively, corresponding to 48% of SBP estimates and 64% of DBP estimates falling into the top grade. In contrast, several models performed worse than the per-subject baseline, with the worst-performing model, CIF+MLP, achieving MASEs of 1.27 and 1.54 for SBP and DBP respectively. Indeed, for DBP estimation only the XResNet1d50+GNLL model achieved an improvement over the subject-

specific baseline, whereas all others performed worse than this baseline. Absolute performance in terms of MAE was better on Calib than CalibFree, as shown by lower MAEs on Calib than CalibFree for all models except the TCN+MLP SBP and DBP models, and the CIF+MLP DBP model. MLP models always performed worse than other models of the same type.

Table 3: The performance analysis for the regression task on the VitalDB CalibFree dataset for three input representations, **T** for raw time series, **F** for feature-based, and **I** for image-based models, next to **B** for the baseline model. The best-performing model is marked in bold-face and underlined, while the second and third best-performing models are highlighted in bold-face for each subset. All MAE values are given in units of mmHg.

Model	SBP MAE (MASE)	IEEE Grades for SBP				DBP MAE (MASE)	IEEE Grades for DBP					
		A	B	C	D		A	B	C	D		
B Baseline	14.87 (1.00)	0.21	0.04	0.04	0.71	9.43 (1.00)	0.33	0.06	0.06	0.55		
T	XResNet1d101	12.70 (0.85)	<u>0.25</u>	0.05	0.05	0.65	8.05 (0.85)	0.39	0.07	0.06	0.48	
	XResNet1d50	12.40 (0.83)	0.24	0.05	0.05	0.66	7.84 (0.83)	0.40	0.07	0.06	0.47	
	Inception1d	14.97 (1.01)	0.21	0.04	0.04	0.71	8.98 (0.95)	0.28	0.05	0.05	0.62	
	LeNet1d	12.37 (0.83)	0.25	0.05	0.05	0.65	7.89 (0.84)	0.39	0.07	0.06	0.47	
	XResNet1d50+GMLA	12.48 (0.84)	0.26	0.05	0.04	0.65	8.16 (0.87)	0.38	0.07	0.06	0.49	
	Alexnet1d	12.34 (0.83)	0.25	0.05	0.05	0.65	7.88 (0.84)	0.39	0.07	0.07	0.47	
	Minirocket	12.35 (0.83)	0.26	0.05	0.05	0.64	7.91 (0.84)	0.39	0.07	0.07	0.47	
	TCN +MLP	12.72 (0.85)	0.25	0.05	0.05	0.65	8.24 (0.87)	0.38	0.06	0.06	0.49	
	F	WAVELET +MLP	14.21 (0.95)	0.22	0.04	0.04	0.70	8.89 (0.94)	0.35	0.06	0.06	0.53
		CIF +GPR	12.90 (0.87)	0.25	0.05	0.05	0.65	8.15 (0.86)	0.38	0.07	0.07	0.48
CIF +MLP		14.02 (0.94)	0.24	0.04	0.04	0.68	8.69 (0.92)	0.36	0.06	0.06	0.52	
I CWT	13.40 (0.90)	0.24	0.05	0.05	0.66	8.39 (0.88)	0.37	0.07	0.07	0.49		

Raw time series (T) and image-based (I) models performed better than feature-

Table 4: Performance analysis for the regression task on the VitalDB Calib dataset for three input representations, **T** for raw time series, **F** for feature-based, and **I** for image-based models, next to **B** for baseline models. The best-performing model is marked in bold-face and underlined, while the second and third best-performing models are highlighted in bold-face for each subset. The subject-specific baseline is used for the calculation of the MASE.

Model	SBP MAE (MASE)	IEEE Grades for SBP				DBP MAE (MASE)	IEEE Grades for DBP					
		A	B	C	D		A	B	C	D		
B	Baseline (global)	14.91 (1.39)	0.21	0.04	0.04	0.71	9.52 (1.65)	0.32	0.06	0.06	0.56	
	Baseline (per subject)	10.72 (1.00)	0.34	0.06	0.05	0.55	5.78 (1.00)	0.56	0.07	0.06	0.30	
T	XResNet1d101	9.08 (0.83)	0.40	0.06	0.06	0.48	6.08 (1.05)	0.53	0.08	0.06	0.32	
	XResNet1d50	9.49 (0.87)	0.37	0.06	0.06	0.51	6.33 (1.08)	0.50	0.08	0.07	0.35	
	Inception1d	9.65 (0.88)	0.36	0.06	0.06	0.54	6.52 (1.11)	0.48	0.08	0.07	0.37	
	LeNet1d	11.61 (1.07)	0.28	0.05	0.05	0.62	7.70 (1.31)	0.40	0.07	0.07	0.46	
	XResNet1d50 +GNLL	7.94 (0.73)	0.48	0.06	0.05	0.41	5.07 (0.87)	0.64	0.06	0.05	0.25	
	Alexnet1d	9.65 (0.88)	0.37	0.06	0.05	0.52	6.21 (1.07)	0.52	0.07	0.06	0.35	
	Minirocket	11.34 (1.05)	0.29	0.05	0.05	0.61	7.41 (1.28)	0.43	0.07	0.06	0.44	
	TCN +MLP	12.84 (1.19)	0.25	0.05	0.05	0.65	8.48 (1.46)	0.37	0.07	0.06	0.50	
	F	WAVELET +MLP	13.62 (1.26)	0.24	0.05	0.04	0.67	8.84 (1.51)	0.36	0.07	0.06	0.51
		CIF +GPR	12.22 (1.13)	0.27	0.05	0.05	0.63	7.78 (1.35)	0.40	0.07	0.07	0.46
CIF +MLP		13.78 (1.27)	0.24	0.05	0.04	0.67	8.94 (1.54)	0.35	0.07	0.06	0.52	
I	CWT	10.23 (0.94)	0.35	0.06	0.06	0.53	6.68 (1.15)	0.50	0.07	0.06	0.37	

based (F) models on Calib (with the one exception of TCN+MLP), as shown by MASEs of 0.73-1.07 (SBP) and 0.87-1.46 (DBP) for raw time series and image-based models, compared to 1.13-1.27 and 1.35-1.54 for feature-based models. There was a less clear difference in performance on CalibFree. Whilst best

performance was achieved with raw time series models, the image-based model performed better than three raw time series models on Calib, and better than one raw time series model on CalibFree. For Calib, more complex models seem to exhibit an advantage (comparing for example XResNet1d50 and XResNet1d101) most likely due to the ability of memorizing subject-specific signal patterns. The only exception from this pattern seems to be the AlexNet1d model, which shows a performance that is almost on par with more complex models and considerably better than comparable lightweight models (such as LeNet1d or TCN+MLP).

Absolute performance in terms of MAE was always better for DBP estimation than SBP estimation. However, when considering errors relative to baseline, MASEs were broadly similar between SBP and DBP on CalibFree, and always higher for DBP than SBP on Calib. Since the IEEE grading system uses absolute errors, performance in terms of IEEE Grades was generally better for DBP than SBP.

4.2 Atrial Fibrillation Detection

Table 5: The performance analysis for the classification task on the DeepBeat dataset for three input representations: **T** for raw time series, **F** for feature-based, and **I** for image-based models. The best-performing model is marked in bold-face and underlined, while the second and third best-performing models are highlighted in bold-face for each subset.

Model	AUC	F1 (0.5)	Specificity (sensitivity > 0.8)	Sensitivity (specificity > 0.8)	MCC (sensi- tivity > 0.8)	MCC (speci- ficity > 0.8)	
T	XResNet1d101	0.86	0.70	0.76	0.73	0.55	0.52
	XResNet1d50	0.87	0.69	0.78	0.78	0.57	0.57
	Inception1d	0.87	0.72	0.79	0.79	0.58	0.58
	LeNet1d	0.76	0.55	0.58	0.50	0.37	0.32
	Alexnet1d	0.84	0.67	0.73	0.71	0.52	0.50
	Minirocket	0.82	0.65	0.68	0.67	0.47	0.47
	TCN+MLP	0.86	0.68	0.74	0.76	0.54	0.54
F	WAVELET + MLP	0.77	0.61	0.59	0.52	0.38	0.33
	CIF+MLP	0.52	0.39	0.20	0.31	-0.002	0.13
I	CWT	0.82	0.69	0.72	0.69	0.50	0.49

Table 5 represents the performance analysis of the classification task (AF/ non-AF) based on the Deepbeat dataset. Similarly to the regression task, raw time series (T) and image-based (I) models performed better than feature-based (F) models in all cases except for the LeNet1d raw time series model, which performed

poorly. The best-performing models were Inception1d and XResNet1d50, which achieved AUCs of 0.87, and F1 scores of 0.72 and 0.69 respectively. As with the regression task, whilst best performance was achieved with the more complex raw time series models, the image-based model performed better than some raw time series models. Whilst feature-based models generally performed worst, wavelet-based features produced better performance than clinically interpretable features.

5 Discussion

5.1 Blood Pressure Estimation

Relative Performance Comparison. For both regression tasks, the best results were achieved by approaches based on raw time series. Feature-based approaches were not competitive in the Calib scenario but are to a certain degree competitive in the CalibFree scenario. Here, it is important to note the differences between Calib and CalibFree: CalibFree tests on unseen patients whereas Calib purposely tests on patients already seen during training, i.e., models can profit to a certain degree from memorization. Quite naturally models achieved much better scores in the Calib setting (even though test sets are not entirely comparable). This also impacts the best-forming models in each of the two settings (within the category of models operating on raw time series). Large and complex models (such as XResNet1d and Inception1d) performed best on Calib, as overfitting to specific patients is desirable, whereas smaller models (such as LeNet1d) performed on par or even better than more complex models in the CalibFree scenario, where generalization to unseen patients is key. This observation aligns with the fact that the gap between raw time series and feature-based approaches is larger in the case of Calib, which is quite natural as this task largely profits from the complexity of the model (and all feature-based approaches are less complex than typical models operating on raw time series).

Comparison to Literature Results. The number of published results on PulseDB is very limited. To the best of our knowledge [46] is the only prior study that reported results on PulseDB, albeit on the full dataset and not just the VitalDB subset, achieving a MAE of 10-11 mmHg for SBP after self-supervised pretraining. We refer to [47] for a recent comparative analysis of different models on different datasets, where models achieved MAEs of between 11 and 19 mmHg for SBP, and between 7 and 11 mmHg for DBP. In comparison, in this study the lowest MAEs were 12.34 and 7.84 mmHg for SBP and DBP respectively on VitalDB CalibFree. This suggests that the presented best-performing models reach state-of-the-art performance.

Impact of Loss Function and Dropout Ensembling. The performance of the XResNet1d50+GNLL in comparison to the XResNet1d50 trained with a regular MAE loss highlights the benefits incorporating dropout ensembling at evaluation, and using a likelihood-based loss can have on model performance.

It suggests that potentially further CNN results could be improved by using a different loss function and ensemble-based evaluation procedure. Interestingly, this only applied to the Calib and not the CalibFree scenario. Other works have reported that modelling uncertainties may improve predictive performance on models trained on ECG data [48]. This variant had two parallel output branches with dropout layers (with a constant but low dropout rate, e.g. 4-5% depending on the task/parameter) dispersed throughout the architecture. Each test input was evaluated 100 times with the dropout layers left active. The predictions produced with the technique are the average of the distribution of outputs produced for each input. Also, a separate model was trained to predict each blood pressure type (systolic/diastolic).

Overall Performance. The best-performing model (XResNet1d50+GNLL on Calib) achieved up to 48% of SBP estimates, and 64% of DBP estimates in the top IEEE category (Grade A), i.e., with prediction errors below 5 mmHg. However, even with this model 41% of SBP estimates and 25% of DBP estimates fell into the lowest category (Grade D). For clinical applications, reducing the fraction of grade D is highly important, or at least identifying patient characteristics that allow to predict whether an unseen patient will belong to grade A or D. This task is referred to as out-of-model-scope detection [49], a task, which is closely related to out-of-distribution detection. Reliable uncertainty estimation is a commonly used approach for the latter and therefore also represents a promising direction for future research. More generally, it might be insightful to assess whether coarser prediction targets, i.e, framing blood pressure prediction as a classification target, could provide clinically meaningful insights, see [50] for an exploration.

Limitations of the VitalDB Dataset. VitalDB is an intraoperative vital signs dataset. Key advantages are that it includes non-cardiac patients, and it is labelled with detailed information on surgical type, surgical approach, anaesthetic type, duration, and device. The dataset covers a wide age range, from neonates to adults. For this study, it was treated as a single dataset, but further disaggregation into subgroups would be essential to identify clinically meaningful features and assess their generalizability in wider healthcare settings. Furthermore, the dataset is not representative of the key application of PPG-based BP monitoring in wearables in the general population, because data were acquired from subjects during surgery rather than in daily life, using clinical pulse oximeters rather than wearable devices.

5.2 Atrial Fibrillation Detection

Relative Performance Comparison. Best performance on the classification case was achieved by modern CNN architectures (XResNet1d, Inception), which performed at least on par with, and in some cases showed advantages over, simpler models (LeNet1d). Feature-based approaches (based on wavelets) showed comparable performance to simple CNNs but were clearly outperformed by large-scale CNNs operating on raw time series input.

Comparison to Literature Results. The original publication describing the DeepBeat dataset [29] reported F1-scores of 0.54 for AF-prediction without pretraining and 0.71 for a multi-task model that jointly predicted AF and signal quality. It is important to stress that these results were achieved on a different, imbalanced split of the dataset and are therefore not directly comparable to those in the present study. The SiamQuality CNN model [46] achieved F1-scores of up to 0.71 on DeepBeat, albeit after self-supervised pretraining. To enable a direct comparison, we trained a XResNet1d50 model on the original split and achieved an F1-score of 0.65, which is clearly superior to the model presented in the original DeepBeat publication. This demonstrates that the presented models reached state-of-the-art performance in comparison to literature benchmarks.

Overall Performance. The best-performing models showed a strong performance in terms of absolute performance values, with F1-scores comparable to or better than reported values in the literature (using the original splits provided by DeepBeat), and sensitivities and specificities of around 0.8. It is worth noting that even though certain commercial AF detection algorithms claim to reach 0.98 sensitivity at >0.99 specificity on internal validation datasets [51], they typically rely on ECG measurements, which serve as the gold standard for AF detection, and severely overestimate the model performance under real-world conditions as the reported performance only applies to certain heart range intervals [52]. In practice, PPG-based AF detection algorithms in consumer wearables are often designed to provide a high positive predictive value by requiring multiple predictions of AF before raising an alert [53, 54] Further work would be required to investigate whether a high positive predictive value could be achieved on real-world data using the models presented in this study.

CIF vs. Raw Time Series Models. The difference in AF detection performance between raw time series models and those based on clinically interpretable features may be influenced by multiple factors, including biases in data acquisition process, artifacts, and even errors in the labelling of recordings into different classes. Deep learning-based raw time series models can use a broad range of information from the signal, enhancing their ability to detect class-specific patterns. However, the drawback is that clinically irrelevant features, such as artifacts and biases, may be incorporated into the training process. In contrast, models that rely on predefined clinically interpretable features, such as pulse irregularity in AF, have a more constrained feature space. While this improves interpretability and robustness in some cases, it may also make these models more vulnerable to mislabelled or noisy data. Initial experiments indicate that incorporating signal quality assessments next to interpretable features can enhance prediction performance. Future work should investigate the classification performance in terms of more fine-grained subgroups, in particular stratified according to signal and labelling quality. Such analysis could reveal if feature-based methods exhibit advantages over raw time series approaches in high-quality subsets, where the underlying assumptions of clinical validity are most clearly satisfied.

Limitations of the DeepBeat Dataset. While the DeepBeat dataset repre-

sents one of the few publicly available PPG-based AF prediction datasets which is large enough for training deep learning models, it is very sparsely documented, and no corresponding ECG signals are available, which would allow one to retrospectively assess the annotation quality. For DeepBeat, three independent cohorts were examined: patients admitted for cardioversion before treatment (classified as AF based on patient ID rather than data window), different participants undergoing exercise stress tests and a challenge dataset as the only subset containing both AF and non-AF samples. Furthermore, the data were categorized into low-, medium-, and high-quality segments, all of which were included in this study. However, there was a notable imbalance, with a greater number of high-quality AF-labelled segments compared to non-AF-labelled segments.

Even though the DeepBeat authors demonstrated the generalization of models trained on DeepBeat to external datasets, due to the substantial differences between these datasets, we cannot conclusively attribute the observed changes solely to AF. The PPG feature variations used to classify the datasets may have resulted from other fundamental differences between them.

5.3 General Insights and Directions for Future Research

General Recommendations on Model Choices. In this study, modern CNN architectures such as XResNet1d provided the best performance in all three cases. Therefore, our general recommendation is to use these modern CNN architectures for prediction models operating on PPG data. However, in certain cases, it may not be necessary to use such complex models (e.g., see the Calibfree scenario of BP regression). Similarly, for certain tasks, models leveraging image representations achieved competitive results. Nevertheless, in the interest of achieving competitive results on an unknown task, the use of modern CNN architectures based on raw time series representations remains the safest choice.

Future Research Directions. An important restriction of the presented study is the restriction to models that were trained from scratch. A very promising extension lies in the consideration of supervised or self-supervised pretraining, which in the case of DeepBeat lead to an increase from 0.71 to 0.91 in terms of F1-scores for the multi-task model. In particular, this applies to the recently published foundation models for PPG data [55, 56]. A second limitation relates to the restriction of assessing the performance purely based on in-distribution performance, which is known to lead to an overly optimistic assessment of the generalization performance. This urges for dedicated studies on the out-of-distribution generalization performance of the presented models, see [57, 58] for first studies in the context of BP prediction. Finally, the entire investigation focused on quantitative assessment of performance, which neglects other quality dimensions such as interpretability, robustness or uncertainty quantification, all of which merit separate investigations.

6 Summary and Conclusion

Our investigations across two exemplary regression and classification tasks found that in general modern CNNs (of the ResNet- or Inception-kind) represented the best-performing approaches. The competitiveness of small-scale models and feature-based approaches depends crucially on the definition of the task at hand. While in some scenarios (e.g. regression CalibFree) they can compete with or in some cases even outperform modern CNNs, they may fail to show competitive performance in other cases (e.g. regression Calib, classification).

The complete implementation, including scripts for data preprocessing as well as model training is available at <https://gitlab.com/qumphy/d1-code>.

7 Acknowledgments

The project (22HLT01 QUMPHY) has received funding from the European Partnership on Metrology, co-financed from the European Union’s Horizon Europe Research and Innovation Programme and by the Participating States. Funding for the University of Cambridge, KCL, NPL and the University of Surrey was provided by Innovate UK under the Horizon Europe Guarantee Extension, grant numbers 10091955, 10087011, 10084125, 10084961 respectively. PHC acknowledges funding from the British Heart Foundation (BHF) grant [FS/20/20/34626].

References

- [1] P. H. Charlton, J. Allen, R. Bailón, S. Baker, J. A. Behar, F. Chen *et al.*, “The 2023 wearable photoplethysmography roadmap,” *Physiol Meas*, vol. 44, no. 11, p. 111001, 2023.
- [2] D. Castaneda, A. Esparza, M. Ghamari, C. Soltanpur, and H. Nazeran, “A review on wearable photoplethysmography sensors and their potential future applications in health care,” *Int J Biosens Bioelectron*, vol. 4, no. 4, pp. 195–202, 2018.
- [3] J. Sola, R. Vetter, P. Renevey, O. Chételat, C. Sartori, and S. F. Rimoldi, “Parametric estimation of pulse arrival time: a robust approach to pulse wave velocity,” *Physiol Meas*, vol. 30, no. 7, p. 603, 2009.
- [4] M. A. Goda, P. H. Charlton, and J. A. Behar, “pyppg: A python toolbox for comprehensive photoplethysmography signal analysis,” *Physiol Meas*, vol. 45, no. 4, p. 045001, 2024.
- [5] C. Ding, R. Xiao, W. Wang, E. Holdsworth, and X. Hu, “Photoplethysmography based atrial fibrillation detection: a continually growing field,” *Physiol Meas*, vol. 45, no. 4, p. 04TR01, 2024.

- [6] C. El-Hajj and P. A. Kyriacou, “Cuffless blood pressure estimation from ppg signals and its derivatives using deep learning models,” *Biomed Signal Process Control*, vol. 70, p. 102984, 2021.
- [7] P. H. Charlton, P. Kyriacou, J. Mant, and J. Alastruey, “Acquiring wearable photoplethysmography data in daily life: The ppg diary pilot study,” *Eng Proc*, vol. 2, no. 1, p. 80, 2020.
- [8] J. C. Nielsen and Group ESD, “2024 esc guidelines for the management of atrial fibrillation developed in collaboration with the european association of cardio-thoracic surgery (eacts),” *Eur Heart J*, vol. 45, no. 36, pp. 3314–414, 2024.
- [9] Group ESD, “2024 esc guidelines for the management of elevated blood pressure and hypertension,” *Eur Heart J*, vol. 45, no. 38, pp. 3912–4018, 2024.
- [10] O. Yildirim, U. B. Baloglu, R. S. Tan, E. J. Ciaccio, and U. R. Acharya, “A new approach for arrhythmia classification using deep coded features and lstm networks,” *Comput Methods Programs Biomed*, vol. 176, pp. 121–33, 2019.
- [11] A. Y. Hannun, P. Rajpurkar, M. Haghpanahi, G. H. Tison, C. Bourn, M. P. Turakhia *et al.*, “Cardiologist-level arrhythmia detection and classification in ambulatory electrocardiograms using a deep neural network,” *Nat Med*, vol. 25, no. 1, pp. 65–9, 2019.
- [12] M. Kachuee, S. Darabi, B. Moatamed, and M. Sarrafzadeh, “Dynamic feature acquisition using denoising autoencoders,” *IEEE Trans Neural Netw Learn Syst*, vol. 30, no. 8, pp. 2252–62, 2018.
- [13] A. Y. Hannun, P. Rajpurkar, M. Haghpanahi, G. H. Tison, C. Bourn, M. P. Turakhia, and A. Y. Ng, “Cardiologist-level arrhythmia detection and classification in ambulatory electrocardiograms using a deep neural network,” *Nature medicine*, vol. 25, no. 1, pp. 65–69, 2019.
- [14] S. Kwon, J. Hong, E. K. Choi, E. Lee, D. E. Hostallero, W. J. Kang *et al.*, “Deep learning approaches to detect atrial fibrillation using photoplethysmographic signals: algorithms development study,” *JMIR MHealth UHealth*, vol. 7, no. 6, p. e12770, 2019.
- [15] P. Cheng, Z. Chen, Q. Li, Q. Gong, J. Zhu, and Y. Liang, “Atrial fibrillation identification with ppg signals using a combination of time-frequency analysis and deep learning,” *IEEE Access*, vol. 8, pp. 172 692–706, 2020.
- [16] B. Aldughayfiq, F. Ashfaq, N. Z. Jhanjhi, and M. Humayun, “A deep learning approach for atrial fibrillation classification using multi-feature time series data from ecg and ppg,” *Diagnostics*, vol. 13, no. 14, p. 2442, 2023.

- [17] T. Pereira, N. Tran, K. Gadhomi, M. M. Pelter, D. H. Do, R. J. Lee *et al.*, “Photoplethysmography based atrial fibrillation detection: a review,” *NPJ Digit Med*, vol. 3, no. 1, pp. 1–12, 2020.
- [18] L. M. Eerikäinen, A. G. Bonomi, L. R. Dekker, R. Vullings, and R. M. Aarts, “Atrial fibrillation monitoring with wrist-worn photoplethysmography-based wearables: State-of-the-art review,” *Cardiovasc Digit Health J*, vol. 1, no. 1, pp. 45–51, 2020.
- [19] R. Ferizoli, P. Karimpour, J. M. May, and P. A. Kyriacou, “Arterial stiffness assessment using ppg feature extraction and significance testing in an in vitro cardiovascular system,” *Sci Rep*, vol. 14, no. 1, p. 2024, 2024.
- [20] R. N. Bracewell, C. Cherry, J. F. Gibbons, W. W. Harman, H. Heffner, E. W. Herold *et al.*, *McGraw-Hill Seires in Electrical and Computer Engineering*. McGraw Hill Boston, 2000.
- [21] S. Mallat, *A wavelet tour of signal processing*. Academic Press, 1999.
- [22] N. E. Huang and Z. Wu, “A review on hilbert-huang transform: Method and its applications to geophysical studies,” *Rev Geophys*, vol. 46, no. 2, p. 2007RG000228, 2008.
- [23] U. Hackstein, T. Krüger, A. Mair, C. Degünther, S. Krickl, C. Schlensak *et al.*, “Early diagnosis of aortic aneurysms based on the classification of transfer function parameters estimated from two photoplethysmographic signals,” *Inform Med Unlocked*, vol. 25, p. 100652, 2021.
- [24] A. Mair, M. Wisotzki, and S. Bernhard, “Classification and regression of stenosis using an in-vitro pulse wave data set: Dependence on heart rate, waveform and location,” *Comput Biol Med*, vol. 151, p. 106224, 2022.
- [25] A. Al Fahoum, A. Al Omari, G. Al Omari, and A. Zyout, “Ppg signal-based classification of blood pressure stages using wavelet transformation and pre-trained deep learning models,” in *2023 Computing in Cardiology Conference (CinC)*, 2023, pp. 1–4.
- [26] J. Wu, H. Liang, C. Ding, X. Huang, J. Huang, and Q. Peng, “Improving the accuracy in classification of blood pressure from photoplethysmography using continuous wavelet transform and deep learning,” *Int J Hypertens*, vol. 2021, pp. 1–9, 2021.
- [27] A. Neshitov, K. Tyapochkin, E. Smorodnikova, and P. Pravdin, “Wavelet analysis and self-similarity of photoplethysmography signals for hrv estimation and quality assessment,” *Sensors*, vol. 21, no. 20, p. 6798, 2021.
- [28] W. Wang, P. Mohseni, K. L. Kilgore, and L. Najafizadeh, “Pulsedb: A large, cleaned dataset based on mimic-iii and vitaldb for benchmarking cuff-less blood pressure estimation methods,” *Front Digit Health*, vol. 4, p. 1090854, 2023.

- [29] J. Torres-Soto and E. A. Ashley, “Multi-task deep learning for cardiac rhythm detection in wearable devices,” *NPJ Digit Med*, vol. 3, no. 1, p. 116, 2020.
- [30] H. C. Lee, Y. Park, S. B. Yoon, S. M. Yang, D. Park, and C. W. Jung, “Vitaldb, a high-fidelity multi-parameter vital signs database in surgical patients,” *Sci Data*, vol. 9, no. 1, p. 279, 2022.
- [31] “Ieee standard for wearable, cuffless blood pressure measuring devices - amendment 1,” *IEEE Std 1708a-2019 Amend IEEE Std 1708-2014*, pp. 1–35, 2019.
- [32] P. Wagner, T. Mehari, W. Haverkamp, and N. Strodthoff, “Explaining deep learning for ecg analysis: Building blocks for auditing and knowledge discovery,” *Comput Biol Med*, vol. 176, p. 108525, 2024.
- [33] H. Ismail Fawaz, B. Lucas, G. Forestier, C. Pelletier, D. F. Schmidt, J. Weber *et al.*, “Inceptiontime: Finding alexnet for time series classification,” *Data Min Knowl Discov*, vol. 34, no. 6, pp. 1936–62, 2020.
- [34] N. Strodthoff, P. Wagner, T. Schaeffter, and W. Samek, “Deep learning for ecg analysis: Benchmarks and insights from ptb-xl,” *IEEE J Biomed Health Inform*, vol. 25, no. 5, pp. 1519–28, 2020.
- [35] B. Lakshminarayanan, A. Pritzel, and C. Blundell, “Simple and scalable predictive uncertainty estimation using deep ensembles,” *Adv Neural Inf Process Syst*, vol. 30, 2017.
- [36] A. Krizhevsky, I. Sutskever, and G. E. Hinton, “Imagenet classification with deep convolutional neural networks,” *Adv Neural Inf Process Syst*, vol. 25, 2012.
- [37] A. Dempster, D. F. Schmidt, and G. I. Webb, “Minirocket: A very fast (almost) deterministic transform for time series classification,” in *Proceedings of the 27th ACM SIGKDD Conference on Knowledge Discovery & Data Mining*, 2021, pp. 248–57.
- [38] S. Bai, J. Z. Kolter, and V. Koltun, “An empirical evaluation of generic convolutional and recurrent networks for sequence modeling,” *arXiv preprint 1803.01271*, 2018.
- [39] P. H. Charlton, P. Celka, B. Farukh, P. Chowienczyk, and J. Alastruey, “Assessing mental stress from the photoplethysmogram: a numerical study,” *Physiol Meas*, vol. 39, no. 5, p. 054001, 2018.
- [40] S. Dash, K. H. Chon, S. Lu, and E. A. Raeder, “Automatic real time detection of atrial fibrillation,” *Ann Biomed Eng*, vol. 37, no. 9, pp. 1701–9, 2009.
- [41] K. Tateno and L. Glass, “Automatic detection of atrial fibrillation using the coefficient of variation and density histograms of RR and Δ RR intervals,” *Med. Biol. Eng. Comput.*, vol. 39, no. 6, pp. 664–671, 2001.

- [42] P. Langley, M. Dewhurst, L. Y. Di Marco, P. Adams, F. Dewhurst, J. C. Mwita *et al.*, “Accuracy of algorithms for detection of atrial fibrillation from short duration beat interval recordings,” *Med Eng Phys*, vol. 34, no. 10, pp. 1441–7, 2012.
- [43] A. Petrėnas, V. Marozas, and L. Sörnmo, *Atrial fibrillation from an engineering perspective*. Springer, 2018.
- [44] C. E. Rasmussen, “Gaussian processes in machine learning,” in *Advanced Lectures on Machine Learning: ML Summer Schools 2003*, O. Bousquet, U. von Luxburg, and G. Rätsch, Eds. Springer, 2004, pp. 63–71.
- [45] H. M. Rai, A. Trivedi, and S. Shukla, “Ecg signal processing for abnormalities detection using multi-resolution wavelet transform and artificial neural network classifier,” *Measurement*, vol. 46, no. 9, pp. 3238–46, 2013.
- [46] C. Ding, Z. Guo, Z. Chen, R. J. Lee, C. Rudin, and X. Hu, “Siamquality: a convnet-based foundation model for photoplethysmography signals,” *Physiol Meas*, vol. 45, no. 8, p. 085004, 2024.
- [47] S. González, W. T. Hsieh, and T. P. C. Chen, “A benchmark for machine-learning based non-invasive blood pressure estimation using photoplethysmogram,” *Sci Data*, vol. 10, no. 1, p. 149, 2023.
- [48] J. F. Vranken, R. R. van de Leur, D. K. Gupta, L. E. Juarez Orozco, R. J. Hassink, P. van der Harst *et al.*, “Uncertainty estimation for deep learning-based automated analysis of 12-lead electrocardiograms,” *Eur Heart J-Digit Health*, vol. 2, no. 3, pp. 401–15, 2021.
- [49] J. Guérin, K. Delmas, R. Ferreira, and J. Guiochet, “Out-of-distribution detection is not all you need,” in *Proceedings of the AAAI conference on artificial intelligence*, 2023, pp. 14 829–37.
- [50] F. Schrumpf, P. R. Serdack, and M. Fuchs, “Regression or classification? reflection on bp prediction from ppg data using deep neural networks in the scope of practical applications,” in *Proceedings of the IEEE/CVF conference on computer vision and pattern recognition*, 2022, pp. 2172–81.
- [51] D. R. Seshadri, B. Bittel, D. Browsky, P. Houghtaling, C. K. Drummond, M. Y. Desai *et al.*, “Accuracy of apple watch for detection of atrial fibrillation,” *Circulation*, vol. 141, no. 8, pp. 702–3, 2020.
- [52] W. Haverkamp, J. Butler, and S. D. Anker, “Can we trust a smartwatch ecg? potential and limitations,” *Eur J Heart Fail*, vol. 23, no. 6, pp. 850–3, 2021.
- [53] S. A. Lubitz, A. Z. Faranesh, C. Selvaggi, S. J. Atlas, D. D. McManus, D. E. Singer *et al.*, “Detection of atrial fibrillation in a large population using wearable devices: The fitbit heart study,” *Circulation*, vol. 146, no. 19, pp. 1415–24, 2022.

- [54] M. V. Perez, K. W. Mahaffey, H. Hedlin, J. S. Rumsfeld, A. Garcia, T. Ferris *et al.*, “Large-scale assessment of a smartwatch to identify atrial fibrillation,” *N Engl J Med*, vol. 381, no. 20, pp. 1909–17, 2019.
- [55] C. Ding, Z. Guo, Z. Chen, R. J. Lee, C. Rudin, and X. Hu, “Siamquality: a convnet-based foundation model for photoplethysmography signals,” *Physiological Measurement*, vol. 45, no. 8, p. 085004, Aug. 2024.
- [56] A. Pillai, D. Spathis, F. Kawsar, and M. Malekzadeh, “Papagei: Open foundation models for optical physiological signals,” *arXiv preprint 2410.20542*, 2025.
- [57] G. Weber-Boisvert, B. Gosselin, and F. Sandberg, “Intensive care photoplethysmogram datasets and machine-learning for blood pressure estimation: Generalization not guaranteed,” *Frontiers in Physiology*, vol. 14, Mar. 2023.
- [58] M. Moulaeifard, P. H. Charlton, and N. Strodthoff, “Generalizable deep learning for photoplethysmography-based blood pressure estimation – a benchmarking study,” *arXiv preprint 2502.19167*, 2025.

A Supplementary material

A.1 Background

A.1.1 Blood pressure estimation

Blood pressure is one of the most widely used physiological measurements. It is a key marker of cardiovascular health; a valuable predictor of cardiovascular events; and is essential for the selection and monitoring of antihypertensive (blood pressure lowering) treatments. However, there are several limitations to blood pressure measurements currently taken in a clinical setting. First, clinical blood pressure measurements are not taken frequently in the wider population, meaning many people around the world are not aware that they have high blood pressure. Second, clinical blood pressures can be unrepresentative of a patient’s normal blood pressure due to the white coat hypertension effect, where a patient’s blood pressure is higher in the clinical setting than normal life. Third, they provide only a snapshot of blood pressure at a single time point, and do not capture diurnal variations which contain important information on health. Fourth, cuff-based blood pressure devices are not suitable for long-term monitoring. Consequently, it would be highly valuable to develop technology to monitor fluctuations in blood pressure, unobtrusively in daily life, such as in wearables.

Photoplethysmography-based blood pressure estimation provides a potential approach to monitor blood pressure unobtrusively in daily life. Photoplethysmography is now widely incorporated into consumer wearable devices, and PPG signals vary with blood pressure. Researchers have focused on two main approaches to estimating blood pressure from PPG signals ¹: (i) using the shape of a single PPG pulse wave; and (ii) using the speed at which the pulse wave propagates through the arteries (the pulse wave velocity). In this project, we focus on the first approach, since it can be implemented in many common wearables such as smartwatches, whereas the second requires simultaneous measurements at different anatomical sites. Blood pressure can potentially be estimated from the shape of the pulse wave using traditional signal processing based on expert-identified features, or using deep learning techniques which learn how the pulse wave is affected by blood pressure changes for themselves.

A.1.2 Atrial fibrillation detection

Atrial fibrillation (AF) is the most common sustained cardiac arrhythmia and confers a five-fold increase in stroke risk. Fortunately, the risk of stroke can be greatly reduced via anticoagulation. However, patients with AF are often underdiagnosed, either because AF episodes occur asymptotically, or because

¹Charlton PH *et al.*, ‘Assessing hemodynamics from the photoplethysmogram to gain insights into vascular age: a review from VascAgeNet’, *American Journal of Physiology-Heart and Circulatory Physiology*, 322(4), H493–H522, 2022. <https://doi.org/10.1152/ajpheart.00392.2021>

it occurs only intermittently and so is not identified during routine testing. Therefore, there is a need for continuous unobtrusive heart rhythm monitoring to identify patients with AF.

Photoplethysmography provides an attractive approach to identifying AF because it is widely used in consumer wearables, and because it provides a measure of the heart rhythm, which is irregular during AF. Indeed, several smartwatches used photoplethysmography to identify irregular rhythms which may be indicative of AF². Irregular heart rhythms have been identified from PPG signals by identifying individual pulse waves corresponding to heartbeats, extracting inter-beat intervals, and assessing the level of inter-beat interval variability, where higher levels of variability indicate higher levels of irregularity. More recently, deep learning models have been developed to identify AF from the PPG signal³.

A.2 Original DeepBeat dataset

This dataset includes over 500,000 signal segments, each with a duration of 25 seconds and a sampling rate of 32 Hz, from 175 individuals, including 108 with atrial fibrillation (AF) and 67 without AF (Table 6). The small test set and the overlapping signal segments of the original dataset affected the analysis. This redundancy led to inflated performance metrics, while the unbalanced distribution of AF and non-AF subjects across training, validation and test sets further biased the results. Consequently, despite its impressive performance on the test set, the original model showed reduced effectiveness on validation and training data. Finally, it is important to note key limitations of this dataset for our study, all signal segments classified as AF were collected from one study protocol where patients came in for a clinical procedure. In contrast, all signal segments classified as non-AF were collected from an independent study where subjects were doing an exercise stress test. Therefore, different devices, human subject parameters (comorbidities, heart rate) would have likely influenced the classification performance, independently of AF. Therefore, confirmatory studies on independent datasets are required before any conclusions about AF classification can be drawn.

Table 6: Original DeepBeat (Stanford Wearable Photoplethysmography) Dataset

Set	Subjects	Total samples	AF samples	Non-AF samples	Data ratio	AF ratio
Train	137	2799784	1269660	1540124	0.839	0.45
Validation	16	518782	47706	471175	0.156	0.09

²Perez, M. V. *et al.* (2019). Large-scale assessment of a smartwatch to identify atrial fibrillation. *New England Journal of Medicine*, 381(20), 1909–1917. <https://doi.org/10.1056/NEJMoa1901183>

³Ding, C. *et al.* (2024). Photoplethysmography based atrial fibrillation detection: A continually growing field. *Physiological Measurement*, 45(4), 04TR01. <https://doi.org/10.1088/1361-6579/ad37ee>

Table 6: Original DeepBeat (Stanford Wearable Photoplethysmography) Dataset

Set	Subjects	Total samples	AF samples	Non-AF samples	Data ratio	AF ratio
Test	22	17617	4230	13387	0.005	0.24

A.3 Performance evaluation and metrics

Blood pressure regression In our blood pressure regression task, we use the L_1 norm to evaluate and compare the performance of the machine learning models. Specifically, we employ the empirical equivalent of this norm, known as the *Mean Absolute Error* (MAE), defined as follows:

$$MAE = \frac{1}{N} \sum_{i=1}^N |y_i - \hat{y}_i|, \quad (1)$$

where y_i denotes the ground truth values, and \hat{y}_i the predictions made by the machine learning model on the test set.

AF classification Detection performance is evaluated by counting the correctly detected AF cases (true positives, N_{TP}), correctly detected non-AF cases (true negatives, N_{TN}), falsely detected AF cases (false positives, N_{FP}), and missed AF cases (false negatives, N_{FN}). Here, the term "case" refers to a segment. Using these four counts, several commonly used performance metrics are calculated.

Sensitivity (Se) describes the probability of a positive result given that the sample is truly positive, i.e.

$$Se = \frac{N_{TP}}{N_{TP} + N_{FN}}. \quad (2)$$

Specificity (Sp) describes the probability of a negative result given that the sample is truly negative, i.e.

$$Sp = \frac{N_{TN}}{N_{TN} + N_{FP}}. \quad (3)$$

The *receiver operating characteristic* (ROC) curve illustrates the performance of a binary classifier at varying threshold values by depicting the rate of truly classified positives against the rate of falsely classified positives. The area *under the curve* (AUC) of the ROC indicates the overall model performance by integrating the ROC over the threshold. The AUC ranges from 0 to 1, with 1 representing perfect detection of positives and negatives and 0 representing perfect misclassification. Moreover, a value of 0.5 represents random classification of the samples. We note that although AUC is widely used, it integrates sensitivity and specificity across both relevant and irrelevant clinical regions and is sensitive to dataset

imbalance^{4,5}. Therefore, it is most useful to understand model performance under different parameter settings during training rather than report general model performance⁶.

The F1 score describes the harmonic mean of the *precision*, i.e., the rate of true positives against the number of all positive labels, and the *recall*, i.e., the rate of true positives against the number of all truly positive samples and describes the overall performance of a classifier. The F1 score is defined via

$$F_1 = \frac{2 N_{TP}}{2 N_{TP} + N_{FP} + N_{FN}}. \quad (4)$$

The F1 score ranges from 0 to 1, with 1 indicating perfect detection and 0.5 indicating performance equivalent to random detection.

The Matthew’s correlation coefficient (MCC) measures the difference between the predicted values of a classifier and the actual class values. MCC is equivalent to the χ^2 -statistics for a 2 x 2 contingency table. The MCC is defined via

$$MCC = \frac{N_{TP}N_{TN} - N_{FP}N_{FN}}{\sqrt{(N_{TP} + N_{FP})(N_{TP} + N_{FN})(N_{TN} + N_{FP})(N_{TN} + N_{FN})}}. \quad (5)$$

In the original form, MCC ranges from -1 to 1, where 1 indicates perfect detection and -1 indicates complete inverse detection. For easier comparison, MCC is typically normalized⁷, however, note that MCC, in contrast to the F1 score, accounts for the number of correctly classified true negatives. MCC is especially useful for imbalanced datasets, as it reflects performance when most AF and non-AF episodes are accurately detected.

In binary classification, the model outputs a raw class confidence value between 0 and 1. However, most evaluation metrics require a binary classified value as input. To classify a sample using the confidence value, we set a classification threshold. If the confidence is below this threshold, the sample is assigned to the negative class; otherwise, it is assigned to the positive class. The threshold is an arbitrary parameter that can be set to achieve the best performance.

For the F1 score, we set the threshold to the naive value of 0.5. The AUC score uses the raw confidence value and does not require a threshold. For the remaining metrics, we choose the threshold that achieves a sensitivity (specificity) on the

⁴Lobo, J. M., Jiménez-Valverde, A., & Real, R. (2008). AUC: a misleading measure of the performance of predictive distribution models. *Global Ecology and Biogeography*, 17(2), 145-151.

⁵Hanczar, B., Hua, J., Sima, C., Weinstein, J., Bittner, M., & Dougherty, E. R. (2010). Small-sample precision of ROC-related estimates. *Bioinformatics*, 26(6), 822-830.

⁶Butkuvienė, M., Petrėnas, A., Sološenko, A., Martín-Yebra, A., Marozas, V., & Sörnmo, L. (2021). Considerations on performance evaluation of atrial fibrillation detectors. *IEEE Transactions on Biomedical Engineering*, 68(11), 3250-3260.

⁷Chicco, D., & Jurman, G. (2020). The advantages of the Matthews correlation coefficient (MCC) over F1 score and accuracy in binary classification evaluation. *BMC genomics*, 21, 1-13.

test set that is closest to, but greater than, 0.8. Once this threshold is set, we calculate the remaining metrics and denote them accordingly.

A.4 Methods

A.4.1 Raw Time Series Models

Researchers have investigated a variety of deep learning models for the prediction of blood pressure using photoplethysmography (PPG) and electrocardiogram (ECG) signals. For instance, a study by Kachuee et al. (2017)⁸ developed a deep neural network model to estimate blood pressure using ECG and PPG signals, which showed significant improvements in accuracy and reliability compared to traditional methods.

Another notable study by Liang et al. (2018)⁹ introduced a hybrid model that integrates CNN and recurrent RNN to exploit both spatial and temporal features of PPG and ECG signals. This model exhibited enhanced performance in continuous blood pressure monitoring, highlighting the potential of deep learning in medical signal processing. It is worth mentioning that transfer learning has been applied to improve the performance of blood pressure prediction models. Zhang et al. (2020)¹⁰ utilized a pre-trained deep learning model and fine-tuned it with a smaller dataset of PPG and ECG signals. This approach minimized the requirement for extensive labelled data, enhancing the practicality of the model for real-world applications.

In this project, we employed prominent models such as LeNet1d¹¹, Inception1d¹², XResNet50d, XResNet101d¹³, AlexNet1d¹⁴ and Minirocket¹⁵ as well as Temporal Convolutional Networks, to conduct a thorough assessment of the outcomes.

⁸Kachuee, M., Kiani, M. M., Mohammadzade, H., & Shabany, M. (2017). Cuffless blood pressure estimation algorithms for continuous health-care monitoring. *IEEE Transactions on Biomedical Engineering*, 64(4), 859-869.

⁹Liang, Y., Chen, Z., Ward, R., & Elgendi, M. (2018). Hypertension assessment via ECG and PPG signals: An evaluation using machine learning models. *Computational and Mathematical Methods in Medicine*, 2018, Article 3179780

¹⁰Zhang, Y., Feng, X., Li, J., Li, B., & Peng, X. (2020). Transfer learning for hybrid deep neural network-based blood pressure estimation. *Journal of Healthcare Engineering*, 2020, Article 5462540.

¹¹LeCun, Y., Bottou, L., Bengio, Y., & Haffner, P. (1998). Gradient-based learning applied to document recognition. *Proceedings of the IEEE*, 86(11), 2278-2324.

¹²Szegedy, C., Liu, W., Jia, Y., Sermanet, P., Reed, S., Anguelov, D., ... & Rabinovich, A. (2015). Going deeper with convolutions. In *Proceedings of the IEEE conference on computer vision and pattern recognition* (pp. 1-9).

¹³Strodthoff, Nils, Temesgen Mehari, Claudia Nagel, Philip J. Aston, Ashish Sundar, Claus Graff, Jørgen K. Kanters et al. "PTB-XL+, a comprehensive electrocardiographic feature dataset." *Scientific data* 10, no. 1 (2023): 279.

¹⁴Krizhevsky, Alex, Ilya Sutskever, and Geoffrey E. Hinton. "Imagenet classification with deep convolutional neural networks." *Advances in neural information processing systems* 25 (2012).

¹⁵Dempster, Angus, Daniel F. Schmidt, and Geoffrey I. Webb. "Minirocket: A very fast (almost) deterministic transform for time series classification." *Proceedings of the 27th ACM SIGKDD conference on knowledge discovery & data mining*. 2021.

Baseline The baseline model predicts blood pressure by using the median value of the blood pressure data, providing a straightforward reference for evaluating the performance of more advanced predictive models.

XResNetd50 /101 XResNet50d and XResNet101d represent deep learning state-of-the-art models derived from ResNet architecture. They incorporate more layers, 50 and 101 layers, respectively, with a number of other enhancements, including group normalization and the option for selective kernel sizes. This allows these models to learn even more intricate hierarchical features and to be very powerful in tasks dealing with complex time-series data. The GNLL variant featured two parallel output branches and dropout layers dispersed throughout the architecture. Separate models were trained for SBP and DBP prediction for each dataset. Each input was evaluated 100 times with dropout layers left active, and the prediction is the mean of the output means.

Inception1d Inspired by the Inception architecture but for one-dimensional signals, it uses parallel convolutional layers with different kernel sizes. This model captures information at multiple scales, enabling the model to understand complex patterns in time series better.

LeNet1d LeNet1 is a one-dimensional convolutional neural network adapted from the original LeNet architecture, which is optimized for time-series data analysis. Considering a greater number of convolutional and pooling layers, it is more appropriate for extracting features from univariate signals, such as PPG or ECG.

AlexNet1d The AlexNet1d is a 1-dimensional adaptation of the popular convolutional neural network (CNN) architecture, traditionally used for 2D image classification. This model consists of two primary components:

1. Feature Extractor: A stacked series of convolutional, ReLU (Rectified Linear Unit), and max pooling layers.
2. Classifier: A fully connected neural network comprising two linear layers, each followed by a ReLU activation function and a dropout layer, to prevent overfitting. The final layer is a linear layer that outputs the model's predictions.

During training, we use the Gaussian negative log likelihood as the cost function, allowing the model to learn the mean and standard deviation of the predictive probability density.

MiniRocket The MiniRocket is an almost deterministic transform for time-series data, followed by a linear classifier. This approach uses dilated convolutions with kernels of length 9 and all possible permutations of the weights -1 and 2 that sum up to 0, where the dilation values are selected to be within a fixed range

relative to the input length. Following the convolution, features are extracted by calculating the proportion of positive values in each convolution output, which is the number of positive values, divided by the sequence length. This process yields a total of 9,996 features, which are then fed into a linear regressor to predict, in our case, the mean and standard deviation of a Gaussian predictive probability density.

The kernels do not require training, allowing for a one-time feature extraction. This enables efficient model training, as only the linear regressor needs to be trained over multiple epochs. This makes the MiniRocket a very fast and effective baseline for time-series classification and regression tasks.

Temporal Convolutional Networks (TCNs) Temporal Convolutional Networks (TCNs) are a class of neural networks designed for sequential data processing. Their ability to capture both short-term and long-term dependencies makes them particularly effective for analyzing complex biological time series signals, such as electrocardiograms (ECGs), electroencephalograms (EEGs), and other physiological measurements. TCNs have been used for both forecasting and classification tasks^{16, 17, 18} yet, to the best of our knowledge, TCNs have never been used for the analysis of PPG signals while we believe TCNs can be relevant for such a task. Indeed, TCNs leverage the strengths of convolutional neural networks (CNNs) and adapt them for temporal data. Unlike recurrent neural networks (RNNs) that process data sequentially, TCNs use convolutional layers to capture temporal dependencies, allowing for parallel processing and typically achieving faster training times. TCNs main features are:

- **Causal Convolutions:** They ensure that predictions at time t are only influenced by inputs from time t and earlier to maintain the temporal order.

$$y(t) = \sum_{i=0}^{k-1} w_i x(t-i)$$

where $x(t)$ and $y(t)$ are respectively the input and output at time t , w_i are the weights of the convolution filter, and k stands for the filter size. This equation ensures that the output $y(t)$ depends only on the current and previous inputs, preserving the causality.

- **Dilated Convolutions:** They allow to capture long-range dependencies using a large receptive field without increasing computational load.

¹⁶Lin, Y., Koprinska, I., & Rana, M. (2020). Temporal Convolutional Neural Networks for Solar Power Forecasting, 2020 International Joint Conference on Neural Networks (IJCNN), Glasgow, UK, 2020, pp. 1-8, doi: 10.1109/IJCNN48605.2020.9206991.

¹⁷Pelletier, C., Webb, G. I., & Petitjean, F. (2019). Temporal convolutional neural network for the classification of satellite image time series. *Remote Sensing*, 11(5), 523.

¹⁸Hewage, P., Behera, A., Trovati, M., Pereira, E., Ghahremani, M., Palmieri, F., & Liu, Y. (2020). Temporal convolutional neural (TCN) network for an effective weather forecasting using time-series data from the local weather station. *Soft Computing*, 24, 16453-16482.

$$y(t) = \sum_{i=0}^{k-1} w_i x(t - d \cdot i)$$

where d represents the dilation factor (which determines the spacing between the elements of the input signal). Dilated convolutions allow the network to cover a larger range of inputs without increasing the number of parameters. Indeed, a dilated convolution lets the network look back up to dk time steps, enabling exponentially larger receptive fields per the number of layers. In the original paper, the authors increased d exponentially with the depth of the network.

- Residual Connections: They help to mitigate the vanishing gradient problem and improve the training of deeper networks.

A.4.2 Clinically Interpretable Feature (CIF)-Based Models

Preprocessing Raw PPG signals often show reduced quality due to motion artifacts, baseline drift, and hypoperfusion. Motion artifacts result from body movement or improper sensor attachment, introducing signal fluctuations that degrade signal quality. Baseline drift, caused by respiration and body movements, shifts the PPG waveform and may obscure the true pulsatile component. Hypoperfusion, characterized by reduced peripheral blood flow due to vasoconstriction, weakens PPG signals, affecting the accuracy and reliability of physiological measurements.

While CNN-based deep learning networks develop custom filter banks during training and require no specific preprocessing, expert-crafted feature-based methods necessitate signal preparation. Typically, the lower bound of the passband (~ 0.5 Hz) removes components below 0.1 Hz and respiratory influences in the 0.1–0.5 Hz range, preserving the AC component. The upper bound (~ 5 –10 Hz) retains primary PPG frequency components, often captured using Butterworth, Chebyshev II, or finite impulse response (FIR) filters.

In this study, for blood pressure estimation, PPG segments from the VitalDB dataset were preprocessed using a Butterworth infinite impulse response zero-phase band-pass filter (4th order, 0.4–7 Hz). For atrial fibrillation detection, PPG segments from the DeepBeat dataset were preprocessed using low-pass, high-pass, and adaptive filters. High-frequency noise and artifacts were removed using a low-pass infinite impulse response filter (cutoff 6 Hz), while baseline wander was eliminated using a high-pass infinite impulse response filter (cutoff 0.5 Hz) and a fifth-order normalized least mean squares adaptive filter with a reference input of unity.

Feature extraction for BP estimation

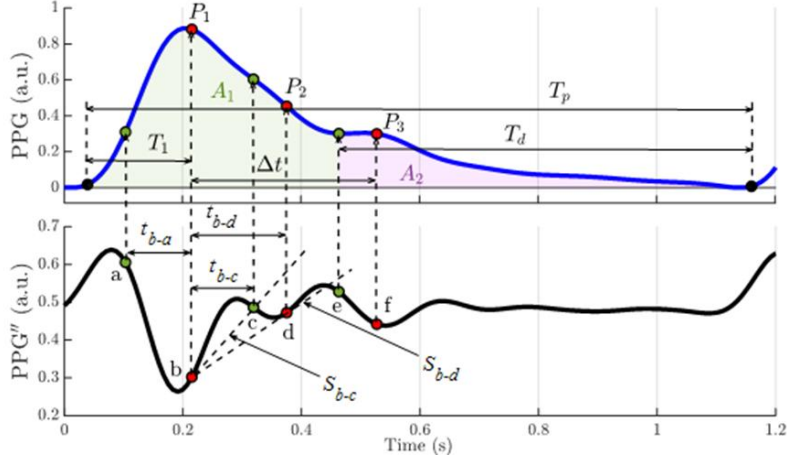


Figure 2: The definition of PPG pulse wave morphology features. Higher-order statistical features extracted from PPG pulse waveforms include skewness and kurtosis, with the latter being the most statistically significant feature for blood pressure estimation.

Clinically Interpretable Features To estimate blood pressure (BP), 28 PPG features¹⁹ were assessed based on pulse morphology analysis and pulse derivative features (Figure 2), which are features selected from the literature²⁴ as the most significant for blood pressure estimation.

PPG pulse wave features include amplitude-related parameters such as the first (P_1) and second (P_2) systolic peaks, the diastolic peak (P_3), and derived indices like the P_2/P_1 ratio, reflection index ($RI = P_3/P_1$), and augmentation index ($AI = (P_1 - P_3)/P_1$). Time-related features consist of the pulse duration (T_p), diastolic duration (T_d), systolic duration (T_1), and the time interval from P_1 to P_3 (Δt). Area-related features include the systolic area (A_1), diastolic area (A_2), the inflection point area ratio ($IPA = A_2/A_1$), and the inflection point area plus the d-wave amplitude of the second PPG derivative ($IPAD$).

PPG derivative features include amplitude-related parameters such as ratios of the second PPG derivative waveform amplitudes (b/a , c/a , d/a , and e/a), the cardiovascular aging index ($AGI = (b-c-d-e)/a$) for arterial stiffness assessment, the interval aging index ($AGI_{int} = (b-e)/a$), and the modified aging index ($AGI_{mod} = (b-c-d)/a$). Time-related features include time intervals between second PPG derivative waves (t_{b-a} , t_{b-c} , t_{b-d}). Slope-related features include the slope coefficients ($slope_{b-c}$, $slope_{b-d}$) of straight lines between amplitudes of b and c , and b and d waves, respectively.

¹⁹Charlton, P. H., Celka, P., Farukh, B., Chowienzyk, P., & Alastruey, J. (2018). Assessing mental stress from the photoplethysmogram: a numerical study. *Physiological measurement*, 39(5), 054001.

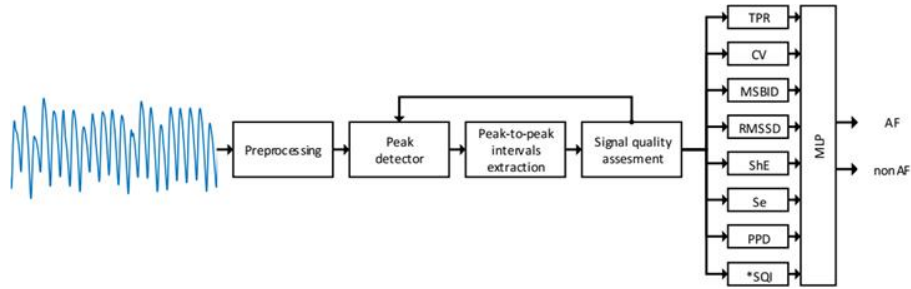


Figure 3: Structure of an MLP-based atrial fibrillation detection using features extracted from the PPG signal.

(Quasi)-periodic signal features To solve the blood pressure regression problem, we employed a Wavelet Packet Decomposition (WPD) approach using the Discrete Wavelet Transform (DWT) for feature extraction from raw PPG-signals. Specifically, we utilized the Daubechies wavelet (db6) of order 3, which offers a balance between time and frequency localization, making it particularly suitable for analysing non-stationary signals.

The wavelet packet decomposition allows for a hierarchical representation of the signal by decomposing both the approximation and detail coefficients at each level. This provides a finer level of signal analysis compared to standard DWT, capturing more detailed information across different frequency bands.

After obtaining the wavelet packet coefficients, these features are flattened and then directly fed, without additional processing, as inputs to a Multi-Layer Perceptron (MLP) model. This simple approach will also be used to diagnose Atrial Fibrillation from PPG-signals.

Feature extraction for AF detection

Irregularity features The irregularities in peak-to-peak (PP) intervals extracted from PPG signals can be evaluated based on measures of randomness, variability, and complexity²⁰. The structure of an MLP-based atrial fibrillation detection algorithm using clinically interpretable features extracted from the PPG signal is shown in Figure 3.

Figure 4 to Figure 7 show PP intervals extracted from 25-s duration PPG segments which are of good quality with AF, good quality without AF, bad quality with AF, and bad quality without AF, respectively.

The following irregularity features are used:

²⁰Petrénas, A., & Marozas, V. (2018). Atrial fibrillation from an engineering perspective (pp. 137-220). L. Sörnmo (Ed.). Berlin: Springer.

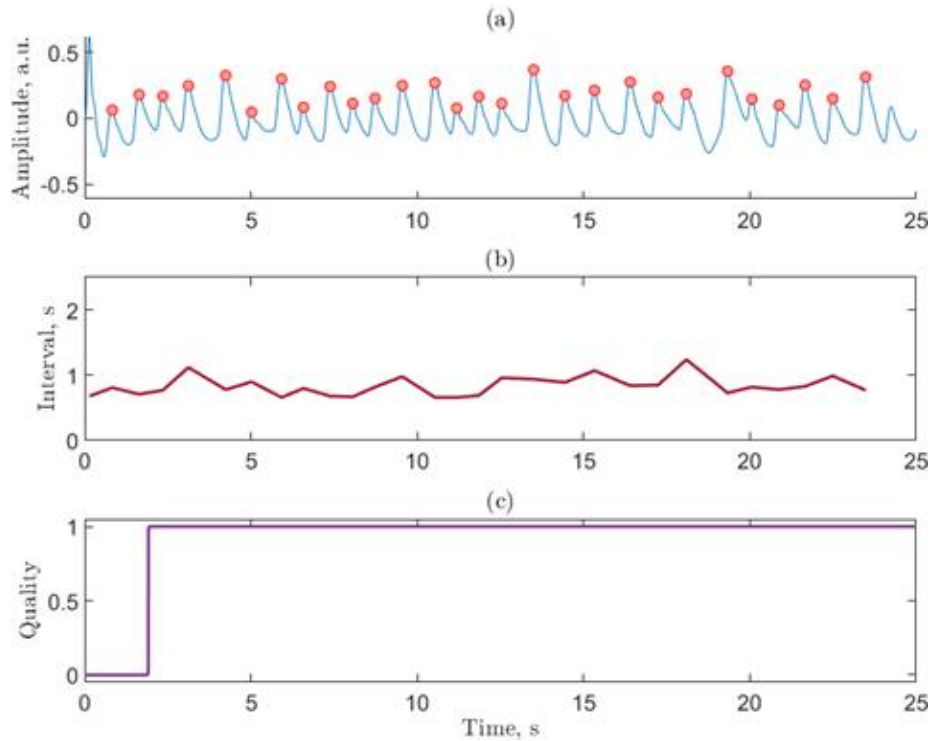


Figure 4: Good-quality AF PPG segment (a) with extracted PP intervals (b) and quality index (c).

- Turning point ratio (TPR)²¹ evaluates randomness in PP intervals by identifying turning points—intervals greater or less than their two neighbours. It is computed as the ratio of turning points to total PP intervals within the analysis window. A higher TPR indicates greater randomness, aiding AF detection.
- Coefficient of variation (CV)^{22,23} relates the standard deviation of PP intervals to their mean. In AF, increased dispersion and decreased mean duration raise CV.
- Mean successive beat interval difference (MSBID)²⁴ also links PP interval

²¹Dash, S., Chon, K. H., Lu, S., & Raeder, E. A. (2009). Automatic real time detection of atrial fibrillation. *Annals of biomedical engineering*, 37, 1701-1709.

²²Tateno, K., & Glass, L. (2001). Automatic detection of atrial fibrillation using the coefficient of variation and density histograms of RR and Δ RR intervals. *Medical and Biological Engineering and Computing*, 39, 664-671.

²³Langley, P., Dewhurst, M., Di Marco, L. Y., Adams, P., Dewhurst, F., Mwita, J. C., ... & Murray, A. (2012). Accuracy of algorithms for detection of atrial fibrillation from short duration beat interval recordings. *Medical engineering & physics*, 34(10), 1441-1447.

²⁴Langley, P., Dewhurst, M., Di Marco, L. Y., Adams, P., Dewhurst, F., Mwita, J. C., ...

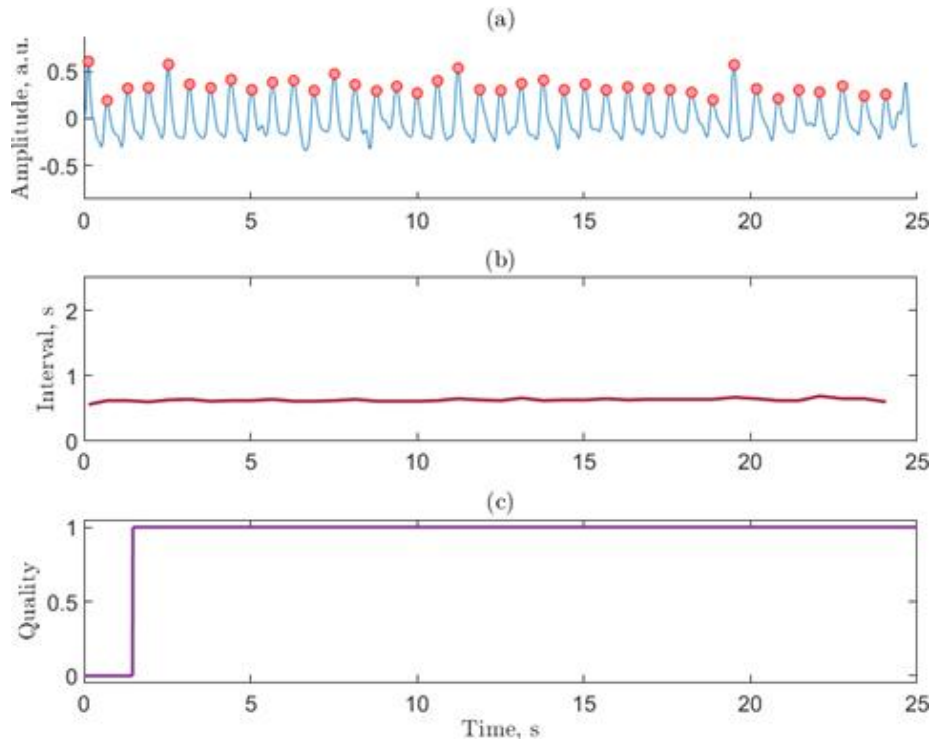


Figure 5: Good-quality AF PPG segment (a) with extracted PP intervals (b) and quality index (c).

dispersion to the mean, similar to CV.

- Root mean square of successive differences (RMSSD)⁵¹ measures dispersion without considering mean heart rate. It typically increases during AF.
- Shannon entropy (ShE)²⁵ quantifies signal unpredictability, rising when distribution is uniform and dropping when centered. ShE is often higher in AF than sinus rhythm.²⁶
- Sample entropy (SE)²⁷ assesses self-similarity by calculating the probability that patterns persist in extended samples. A simplified SE is used here for

& Murray, A. (2012). Accuracy of algorithms for detection of atrial fibrillation from short duration beat interval recordings. *Medical engineering & physics*, 34(10), 1441-1447.

²⁵Shannon, C. E. (1948). A mathematical theory of communication. *The Bell system technical journal*, 27(3), 379-423.

²⁶Zhou, X., Ding, H., Ung, B., Pickwell-MacPherson, E., & Zhang, Y. (2014). Automatic online detection of atrial fibrillation based on symbolic dynamics and Shannon entropy. *Biomedical engineering online*, 13(1), 1-18.

²⁷Richman, J. S., & Moorman, J. R. (2000). Physiological time-series analysis using approximate entropy and sample entropy. *American journal of physiology-heart and circulatory physiology*, 278(6), H2039-H2049.

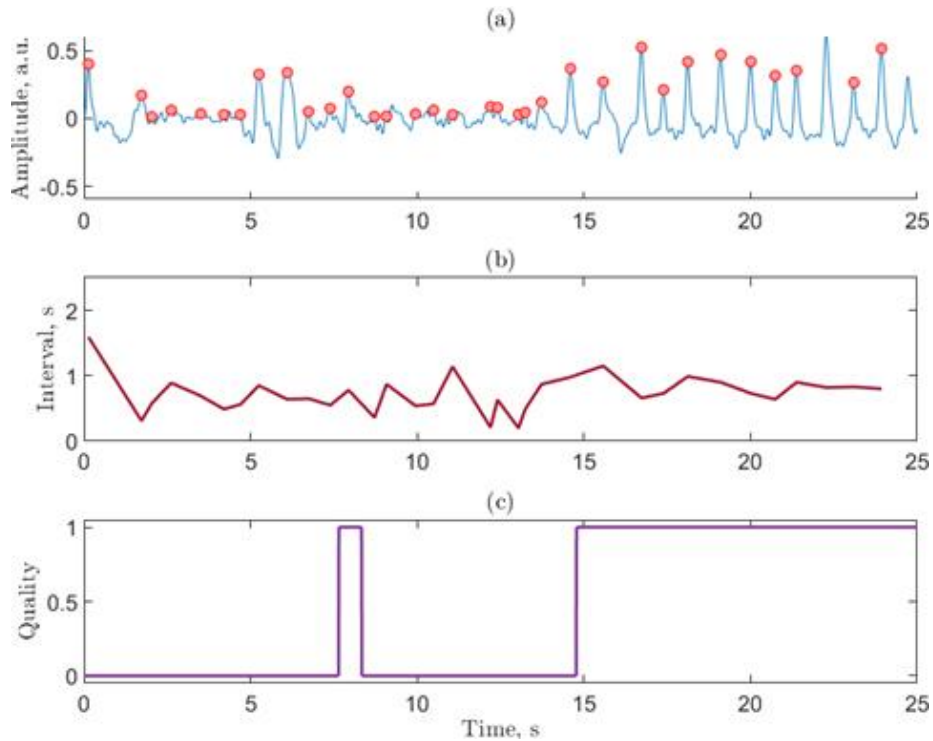


Figure 6: Bad-quality AF PPG segment (a) with extracted PP intervals (b) and quality index (c).

efficient AF detection.²⁸

- Poincare plot (PPD)^{29,30} visualizes consecutive PP intervals. In AF, it shows significantly greater dispersion compared to sinus rhythm or ectopic beats.

The capacity of each feature to discriminate between AF and non-AF cases is depicted in Figure 8 and Figure 9. Figure 8 shows separation of features before the removal of bad-quality PPG segments, while Figure 9 shows separation of features after the removal of bad-quality PPG segments. PPG signal quality assessment was performed using the algorithm described in³¹. The best visible

²⁸Petrėnas, A., Marozas, V., & Sörnmo, L. (2015). Low-complexity detection of atrial fibrillation in continuous long-term monitoring. *Computers in biology and medicine*, 65, 184-191.

²⁹Park, J., Lee, S., & Jeon, M. (2009). Atrial fibrillation detection by heart rate variability in Poincare plot. *Biomedical engineering online*, 8(1), 1-12.

³⁰Lian, J., Wang, L., & Muessig, D. (2011). A simple method to detect atrial fibrillation using RR intervals. *The American journal of cardiology*, 107(10), 1494-1497.

³¹Sološenko, A., Petrėnas, A., Paliakaitė, B., Sörnmo, L., & Marozas, V. (2019). Detection of atrial fibrillation using a wrist-worn device. *Physiological measurement*, 40(2), 025003.

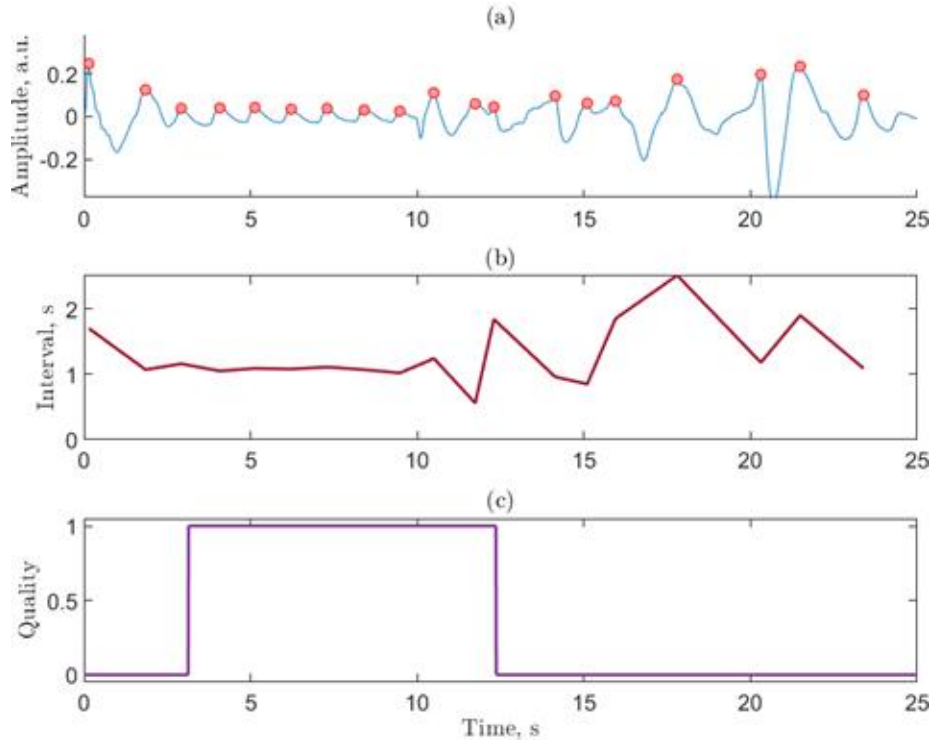


Figure 7: Bad-quality AF PPG segment (a) with extracted PP intervals (b) and quality index (c).

separation of features is achieved by using SE and PPD, especially when estimated bad-quality segments are removed.

Models

Multilayer perceptron models The multilayer perceptron (MLP) used for classifying features extracted from PPG signals consists of a fully connected layer with 128 neurons, followed by a ReLU activation function and a dropout layer with a 0.5 dropout rate for regularization. The network's output structure includes a fully connected layer with 2 neurons, a softmax layer to produce a probability distribution for multi-class classification, and a classification layer for determining the final class label. The model is trained using the Adam optimization algorithm, with fixed learning rate of 0.01 and mini-batch size of 32.

Gaussian process regression Gaussian Process Regression (GPR) is a powerful and flexible non-parametric regression technique used in machine learning

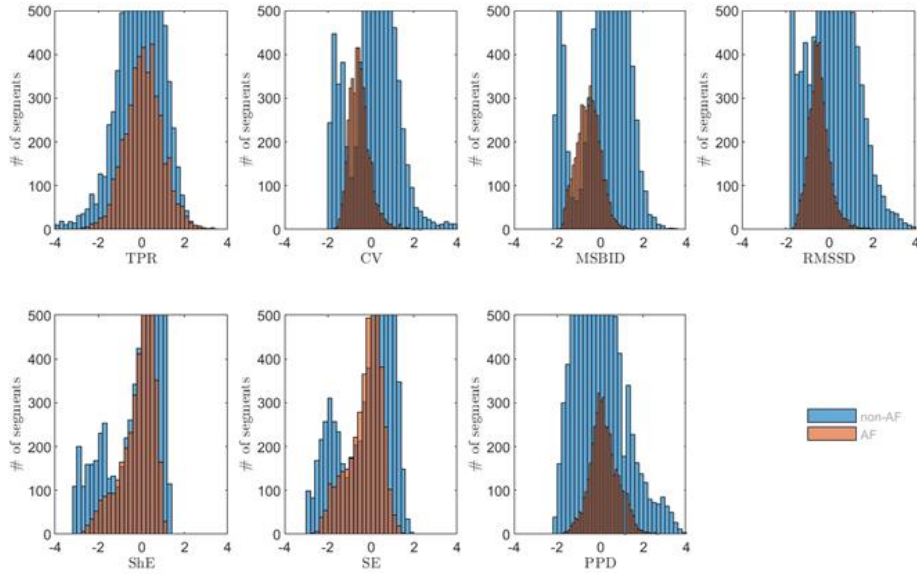


Figure 8: Discriminative capacity of each feature to distinguish between AF and non-AF cases without removing bad-quality PPG segments.

and statistics for modeling complex, nonlinear relationships³². Instead of fitting a specific function to the data, GPR models the relationship between input features and output as a distribution over functions. It incorporates prior knowledge (expressed through kernels) and provides uncertainty estimates for individual predictions. The objective of GPR is to find a mean function that accurately represents observed data points and can be used for predicting new data points. Gaussian Processes define a distribution over an infinite number of potential functions that could fit the data.

The key points of the GPR method include the use of the Fully Independent Conditional (FIC) approximation for making predictions given the model parameters and the squared exponential kernel as the covariance function. The inter-point distance computation for evaluating built-in kernel functions was specified as the training function $(x - y)^2$. To ensure accurate parameter estimation, a QR-factorization-based approach was employed for computing the log-likelihood and gradient. Additionally, the limited-memory Broyden-Fletcher-Goldfarb-Shanno (LBFGS) optimizer was used for hyperparameter estimation. As a quasi-Newton method, LBFGS approximates the Hessian matrix using past gradient information, enabling rapid convergence in high-dimensional parameter spaces while maintaining computational feasibility and numerical stability. The combination of QR-factorization, the squared exponential kernel, a linear basis

³²Rasmussen, C. E. and C. K. I. Williams. Gaussian Processes for Machine Learning. MIT Press. Cambridge, Massachusetts, 2006.

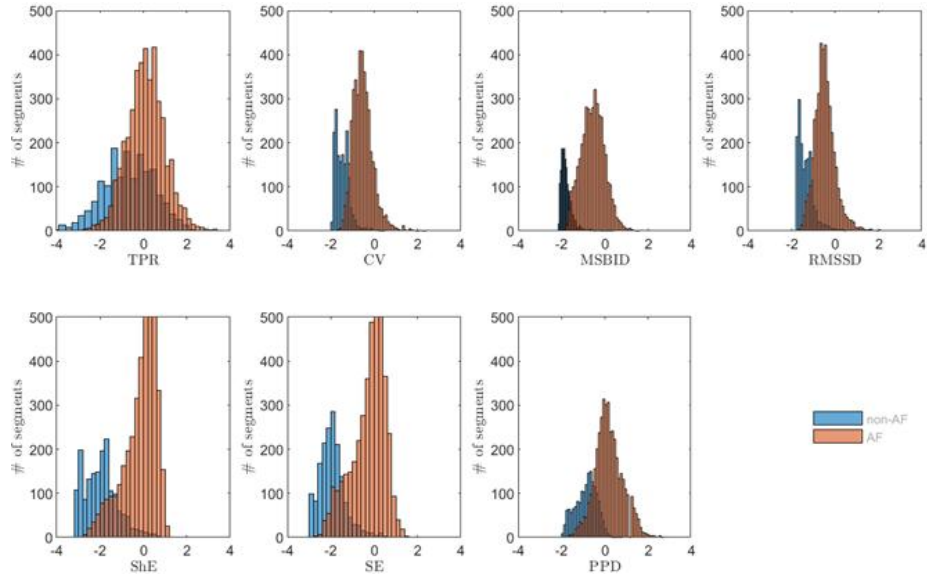


Figure 9: Discriminative capacity of each feature to distinguish between AF and non-AF cases using the removal of bad-quality PPG segments.

function, and the FIC approximation enhances the predictive performance and scalability of the model.

A.4.3 Image-Based Models

Continuous Wavelet Transform (CWT) image representations CWT transformation requires to define several hyperparameters among which the most important are the (1) the choice of the wavelet function, (2) the number of scales and, (3) the window size for the wavelet function at each scale. Indeed, scales affect the frequency resolution, higher scales focusing on lower frequencies and longer time windows. The number of scales defines how many different frequency bands the CWT will compute. In this project, we use a generalized morse wavelet (GMW) as the mother wavelet with a length of 1024 and 128 logarithmically spaced scales. Applying the CWT transform to PPG signals with shape $(\langle \text{sequence_length} \rangle, 1)$ yields a 2D array with size $(\langle \text{sequence_length} \rangle, 128)$ which is saved as an RGB image.

State-of-the art methods relying on CWT based scalogram as inputs, feed the CWT images to a deep learning model to perform classification/regression tasks. We propose to use the same model (ResNet18) for both blood pressure estimation and Atrial Fibrillation detection, the only difference being the addition of a sigmoid function for Atrial Fibrillation detection.

The only input preprocessing step simply consists in resizing CWT images into

squared RGB images with shape $(224,224,3)$. Such input size is typically dictated by the availability of pre-trained models commonly trained on the ImageNet dataset.